



FINITE ELEMENT ANALYSIS OF POLYMER-BASED OPTICAL INTERCONNECTS

STUDENT PROJECT

Hannover center for optical technologies- Leibniz University of Hannover

By

Murat Baran

04.05.2020

Project duration	300 Hours
Matriculation number	10018117
Working institute	Hannover center for optical technologies
Mentor	Monali Suar

ABSTRACT

Thermal, deformation, and optical simulations are performed on polymer PMMA waveguide at different temperatures by using FEM (Finite Element Method). The models which are used in the simulations aim to calculate the heat distribution and thermally induced mechanical stress. The microheater is implemented at the top of the waveguide and inside the top cladding to analyze the thermo-optic effect on the waveguide. We found that the microheater is more effective and causes a uniform thermal distribution in the core. Also, this thermal effect results in a change of refractive index which is analyzed in this paper. It is found that the mechanical stress on the waveguide affects the shape and the index of refraction of the waveguide. Hence, it plays a role in the optical performance. Shear stress has little effect on the waveguide along the propagation axis, because we fixed the waveguide from the sides.

Keywords: Polymer waveguide, monomer, microheater, thermo-optic effect, thermal simulation, optical simulation, FEM, stress, stress-Optical Effect

ACKNOWLEDGMENTS

I would like to thank my advisors Prof. Dr. Bernhard Wilhelm Roth and M. Sc. Monali Suar for their mentorships, supports and helps. Their extensive and intensive knowledges and precisions in science and research consistently whenever I needed, providing me a warm working atmosphere and kindness in life deeply impressed me, and I believe that I will benefit greatly from this experience in my future endeavors.

I also appreciate the help from my classmate Zulqarnain Sheikh and all the other people in my department whoever helped me.

Finally, I would like to thank my wife, my son, and my parents for their love, support and encouragement. They are there for me whenever I need them the most.

LIST OF VIDEOS

Video 1. Thermal distribution for model 1	20
Video 1. Thermal distribution for model 2	20

LIST OF TABLES

Table 1. The parameters used in the thermal simulation	17
Table 2. The parameters used in the stress and deformation analysis	18

LIST OF FIGURES

Figure 1.1 A model wall	9
Figure 2.1 Processes leading to fabrication of advanced engineering systems.	13
Figure 2.2 Main graphical user interface (GUI) window	14
Figure 2.3 Typical data and methods in the procedure of finite element analysis modeling	14
Figure 2.4 Geometry of model 1	15
Figure 2.5 Geometry of model 2	16
Figure 2.6 An example of unstructured grid for a finite element analysis mesh	16
Figure 2.7. a Mesh of model 1	16
Figure 2.7. b Mesh of model 2	17
Figure 2.8 Boundaries of model 1	18
Figure 2.9 Boundaries of model 2	18
Figure 3.1. a Model 1	20
Figure 3.1. b Model 2	20
Figure 3.2. a Temperature-Time graph for model 1	21
Figure 3.2. b Temperature-Time graph for model 2	21
Figure 3.3. Thermal distribution along L1 for the models	21
Figure 3.4. a Temperature distribution for model 1	22
Figure 3.4. b Temperature distributions for model 2	22
Figure 3.5. a Deformation distribution for model 1	22
Figure 3.5. b Deformation distribution for model 2	23
Figure 3.6. a Displacement-Length graph in x-axis for model 1	23

Figure 3.6. b Displacement-Length graph in x-axis for model 2	23
Figure 3.7. a Displacement-Length graph along L1 for model 1	23
Figure 3.7. b Displacement-Length graph along L1 for model 2	23
Figure 3.8. a Refractive index change-Length graph along L1 for model 1	24
Figure 3.8. b Stress-Length graph along L1 for model 1	24
Figure 3.9. a Refractive index change-Length graph along L1 for model 2	24
Figure 3.9. b Stress-Length graph along L1 for model 2	24
Figure 3.10. a Transverse electric mode without heating for model 1	25
Figure 3.10. b Transverse magnetic mode without heating for model 1	25
Figure 3.11. a Refractive index-Temperature graph for the core and the cladding for model 1	25
Figure 3.11. b Refractive index-Temperature graph for the core and the cladding for model 2	25

TABLE OF CONTENTS

ABSTRACT	II
ACKNOWLEDGMENTS.....	III
LIST OF VIDEOS	IV
LIST OF TABLES.....	IV
LIST OF FIGURES.....	IV
CHAPTER 1.....	7
INTRODUCTION	7
1.1. THEORETICAL BACKGROUND	9
1.1.1. <i>Heat Conduction Analysis</i>	9
1.1.2. <i>Stress Analysis</i>	10
1.1.3. <i>Thermo-optic Simulation Theory</i>	12
CHAPTER 2.....	13
MODEL & METHOD.....	13
2.1. WHAT IS FEATool MULTIPHYSICS?	13
2.2. MULTIPHYSICS MODE.....	15
2.2.1. <i>Selecting the Dimension</i>	15
2.2.2. <i>Geometrical Design</i>	15
2.2.3. <i>Mesh Generation</i>	16
2.2.4. <i>Definition of the Equations</i>	17
2.2.5. <i>Boundary Conditions</i>	18
2.2.6. <i>Solving/Computing of the Problem</i>	19
2.2.7. <i>Visualization/Postprocessing of the Result</i>	19
CHAPTER 3.....	20
RESULTS.....	20
3.1. THERMAL SIMULATION.....	20
3.2. STRESS AND DEFORMATION ANALYSIS.....	22
3.3. THERMO-OPTIC SIMULATION AND ANALYSIS.....	24
CHAPTER 4.....	26
CONCLUSION	26
REFERENCES	27

Chapter 1

Introduction

Planar polymer waveguides have attracted extensive attention for their applications in telecommunication and data communication [1,2], because of the low cost, simple processes, and high thermo-optic coefficient of polymers. Various photonic devices, such as the thermal optical switches (TOS) [3,4], variable optical attenuators (VOA) [4–6], optical couplers/splitters [7], and arrayed waveguide gratings (AWG) [8,9], were fabricated using polymer waveguides. While the basic optical properties of polymers, including optical loss, refractive index, birefringence, are critical for using polymers to fabricate quality waveguide devices, the thermo-optic (TO) coefficient of polymers plays a vital role in determining the device performance [10]. On the other hand, it causes a major drawback for thermal stability in some devices, such as an AWG. In such devices, the operating conditions may easily drift with the change of device's refractive index due to the exposure of environmental changes during field service [11].

In many cases, the overall device performance can be limited by the thermal response of the structure. For example, the switching time depends on the rate of heat dissipation generated by the heating electrode. Such heat dissipation not only depends on the waveguide materials but also on the size and shape of the waveguide and heater [12].

Thermal properties of polymers are rather different compared to glasses. Service temperature limits for polymers (60 to 250 °C) are substantially less than for optical glasses (400 to 700 °C) [13]. The thermal expansion coefficient is about one order of magnitude greater than glass. For example, the linear thermal expansion coefficient of Acrylic has average value of $7 \times 10^{-5} \text{ K}^{-1}$ [14] while for the N-BK7 glass the corresponding value is $0.71 \times 10^{-5} \text{ K}^{-1}$ [15]. Now-a-days many approaches are used to control light beams in optical waveguide devices which are ground based on thermo-optic (TO) effects. According to Nishihara *et al.* [16], TO effect is a way in which the material refractive indices depend on the temperature. It utilizes the temperature dependence of the refractive index dn/dT . The change of this parameter depends on two counteracting effects: the change in density caused by positive coefficient of thermal expansion and the increase in polarizability with temperature. Evaluation of dn/dT is possible by differentiation of the Lorentz-Lorenz equation with respect to temperature. The temperature gradient of refractive index dn/dT is referred in literature as a thermo-optic coefficient [17] or temperature coefficient of refractive index [14]. The absolute values of dn/dT of polymer materials are with orders of magnitude larger than those for optical glasses and exhibit usually negative deviations compared to the positive thermo-optic coefficients for most of glasses. Small thermally-induced changes of the refractive index can significantly alter the light-intensity distribution within waveguides, especially in coupled systems [18]. A large refractive index change for low input power is critical for creating practical devices [19]. Also, low cost materials can be made, even though it is difficult, out of the polymer material which have sufficiently large nonlinear susceptibilities [20-21].

Internal stress into optical waveguides is introduced by this research. Compressive or tensile stress can be introduced in a direction which is either parallel or perpendicular to

the direction of optical propagation. The existence phenomenon as the stress-optical effect can cause changes in the polymer refractive index through the photo-elastic effects. The waveguide becomes strained during the fabrication processes. This is caused, because of the difference of the thermal expansion coefficients of the core and the cladding of the materials. This stress will cause the indices to become anisotropic and increases the birefringence in the waveguide. In modern optical systems, more and more components are integrated (or hybrid-packaged) in a single chip, where optical waveguides serve as interconnects for photonic components. Due to fabrication and packaging, stresses cannot be avoided in these complicated structures with many diverse materials. These stresses can change the refractive indexes of the waveguide by the acousto-optic (elasto-optic or photoelastic) effect [22] (Xu and Stroud, 1992; Sapriel, 1979), which may affect the optical performance which has been observed in photoelectric devices. [23]

Internal stress into optical waveguides is introduced by this research. Compressive or tensile stress can be introduced in a direction which is either parallel or perpendicular to the direction of optical propagation.

In our study, thermal, deformation, and optical simulations are carried out for the top and the buried models accomplished by using finite element method (FEM) via FEATool and COMSOL multiphysics softwares. Many articles around 50 about the simulations and analysis mentioned above are examined and the most important points taken as references to the study. In section 1, thermal simulation for the upper and the buried micro-heaters are carried out by using FEM via FEATool. Analysis of temperature distributions in the waveguide as a result of applied heat or known as thermal analysis is performed. The thermal distribution is used as an indicator to how the refractive index changes in the waveguide structure as demonstrated by Moller et al. [24], Sircilli et al. [25] and Wang et al. [26]. The basic idea of thermal analysis is to solve the heat equation as described by Kokkas [25] in his work on multiple-layer structure. Various methods have been used to solve this equation which include the finite difference method [24], finite element method [27] and Fourier Transform method [26]. Electric heating is chosen to be the driving method because electric microheaters can be easily fabricated into a switching structure using microfabrication techniques, which allows for simple and accurate control. [28] The deformed waveguide is drawn visually in section 2. Also, deformation in the x axis and elongation in the z propagation axis are calculated and plotted. The thermo-optical simulation is performed and the relationship between the temperature and the index of refraction of the cladding and the core for certain points is examined and illustrated by the graphs and images in section 3, after obtaining the refractive index distribution through the thermo-optic effect where the temperatures of the heater is set from 20 to 200 °C range. Ambient temperature surrounds the waveguide. By this research, it is aimed to tune the index of refraction. So, in this way, thermally tunable devices can be made.

1.1. Theoretical Background

In this part, the theoretical background of the thermal, stress, and optical simulations utilized in the project will be explained.

1.1.1. Heat Conduction Analysis

Conduction is the heat transfer through an object by the means of its molecules. A temperature gradient or slope is settled down by the energy which is constantly being transported in the direction of decreasing temperature.

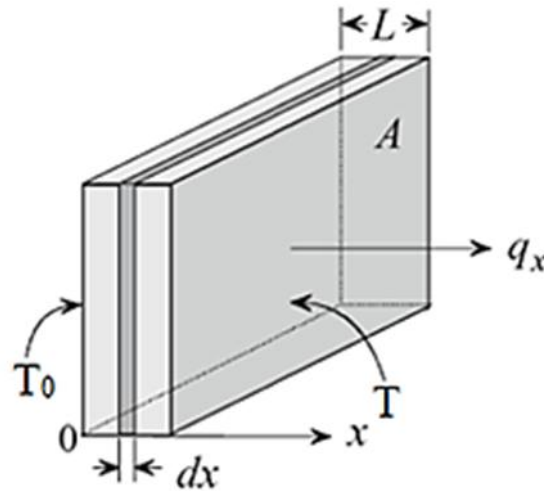


Fig. 1.1 A model wall [29]

Now, a law can be formulated which helps us to determine the rate of heat through conduction. A wall is considered as shown in the figure 1.1. The coordinate system starts from the bottom left corner which is (0, 0). The temperature of the surface of the wall on the left is T_0 and the other side temperature is T . The wall thickness is L and the surface area is A . The other surfaces are assumed as insulated and the direction of the heat is in the x -direction only. Assume steady state and q_x be the rate of heat transfer. It is obtained from the experiments that q_x is directly proportional to A and $(T_0 - T)$ and inversely proportional to L

$$q_x \propto \frac{A(T_0 - T)}{L}$$

Proportionality constant is added and the formula below is obtained

$$q_x = \frac{A(T_0 - T)}{L} \quad (1.1)$$

Where k is the thermal conductivity. In order to use equation (1.1), 3 conditions must be met. They are steady state, constant k , and conduction in one dimension. The formula should be rewritten which contains these limitations. If equation (1.1) is implemented to the element dx , T_0 becomes $T(x)$, T turns into $T(x+dx)$, and L is replaced by dx . The new formula is

$$q_x = k A \frac{T - T(x + dx)}{d} = -k A \frac{T(x + dx) - T}{d}$$

The change in T is dT which can be found by $T(x+dx) - T_x$, so the formula become

$$q_x = -k A \frac{d}{d} \quad (1.2)$$

The term heat flux, q'_x which indicates the amount of heat per unit area normal to x. So,

$$Q'_x = \frac{q_x}{A} \quad (1.3)$$

Now, equation (1.2) can re-written as below

$$Q'_x = -k \frac{D}{d} \quad (1.4)$$

Despite equation (1.4) is made for the conduction in one dimension, it can be generalized for three dimension and also for transient conditions. It should be noted that heat flow is a vector quantity. In order to reflect the direction of the heat flow, the derivation in the equation (1.4) is converted into a partial derivation as follows:

$$Q'_x = -k \frac{\partial T}{\partial x}, \quad q'_y = -k \frac{\partial T}{\partial y}, \quad q'_z = -k \frac{\partial T}{\partial z} \quad (1.5)$$

where x, y, and z represent the coordinates. The equation above Eq. 1.5 is known as Fourier's law of conduction. Three observations are worth making: (i) the negative sign indicates that when the gradient is negative, heat flow is in the positive direction, i.e., towards the direction of decreasing temperature, as dictated by the second law of thermodynamics. (ii) The conductivity k need not be uniform since equation (1.5) applies at a point in the material and not to a finite region. In reality the thermal conductivity varies with temperature. However, equation (1.5) is limited to isotropic material, i.e., k is invariant with direction. (iii) Returning to our previous observation that the focal point in conduction is the determination of temperature distribution, we now recognize that once $T(x, y, z, t)$ is known, the heat flux in any direction can be easily determined by simply differentiating the function T and using equation (1.5) [29].

1.1.2. Stress Analysis

The finite element method was originally developed for the stiffness analysis of airplane [30]. Stress analysis is one of the most used modules of FEM. Consequently, stress analysis is the most typical application of FEM. Generally, it is well known that the total potential energy should be a minimum when thermal stress and/or an external force is applied to the body. In other words, the strain distribution that is actually generated among all possible strain profiles is the distribution that makes the potential energy a minimum. This is called the energy principle [31]. The total potential energy of the body is given by

$$\Pi = (\text{internal work}) - (\text{external work}) = U - V \quad (1.6)$$

where U and V denote strain energy and work done by the external force; respectively Strain energy U is work generated during the process of releasing strain; that is, U is a summation of {local force generated under certain strain condition} \times {displacement by the force}. Since potential energy decreases by the amount of work done by the external force, V in equation (1.6) has a minus sign [32].

The method where stress analysis is based on energy principle known as energy method. Energy method's calculation procedures are summarized by the steps as follows:

1. Shows the potential energy in terms of the displacement by strain and an external force.
2. Find the approximations of the displacement and the external force in the inward or outward directions for each element by the help of analytical functions using values at nodal points.
3. Apply the energy principle to the potential energy which makes partially differentiated with the respect to the displacement and form an equilibrium equation called as linear simultaneous equation.
4. Determine the displacement for each nodal point by solving the simultaneous equation.
5. Calculate the strain and the stress for each element by using displacements at the nodes which surrounds the element.

In three-dimensional FEM analysis, it is necessary to have a computer with a large memory, because it takes a long processing time for the calculations. That is why two-dimensional FEM analysis is often preferred to be used. An appropriate assumption is made for each problem.

Now, an object will be taken which is longer in its y-axis than its cross-sectional area. This suits the waveguide used in the project perfectly. Then, the strain in the object along the y-axis is taken as 0.

$$\epsilon_y=0 \quad (1.7)$$

Stress analysis based on the assumption used above is called as *plane strain problem*. Beside this, the stress component σ_y which is normal to the plane is considered as zero

$$\sigma_y=0 \quad (1.8)$$

The basic equations for the displacement, stress, and strain will be discussed now where u and v are the displacement along the x- and z-axis directions respectively, ϵ_x , ϵ_y , and ϵ_z are the principal strains along x-, y-, and z-axis directions respectively, γ_{xz} is the shear strain in the x-z plane, σ_x , σ_y , and σ_z are principal stresses along x-, y-, and z-axis directions respectively, τ_{xz} is the shear stress in the x-z plane, f and g are the external forces along x- and z-axis directions respectively. E and ν are the Young's modulus and Poisson's ratio respectively.

The relationship between displacement and strain is given by [33]

$$\epsilon_x = \frac{\partial u}{\partial x}, \quad (1.9a)$$

$$\epsilon_z = \frac{\partial v}{\partial z}, \quad (1.9b)$$

$$\gamma_{xz} = \frac{\partial u}{\partial z} + \frac{\partial v}{\partial x}. \quad (1.9c)$$

In the next step, the stress-strain relationship is generally expressed as

$$\epsilon_x = \frac{1}{E} [\sigma_x - \nu(\sigma_y + \sigma_z)] + \alpha, \quad (1.10a)$$

$$\epsilon_y = \frac{1}{E} [\sigma_y - \nu(\sigma_z + \sigma_x)] + \alpha, \quad (1.10b)$$

$$\epsilon_z = \frac{1}{E} [\sigma_z - \nu(\sigma_x + \sigma_y)] + \alpha, \quad (1.10c)$$

$$\gamma_x = \frac{\tau_x}{G} = \frac{2+(1+\nu)}{E} \tau_x . \quad (1.11)$$

where G is the shear modulus, α is the thermal expansion coefficient, and ΔT is the change in temperature respectively. The plain stress problem can be found if the equation (1.7) in the equation (1.10) is substituted. So, the plane strain problem is found by

$$\sigma_x = \frac{E}{(1+\nu)(1-2\nu)} [(1-\nu)\epsilon_x + \nu\epsilon_y] - \frac{\alpha}{(1-2\nu)} \Delta T, \quad (1.12a)$$

$$\sigma_y = \nu(\sigma_x + \sigma_z) - \alpha \Delta T, \quad (1.12b)$$

$$\sigma_z = \frac{E}{(1+\nu)(1-2\nu)} [(1-\nu)\epsilon_x + \nu\epsilon_z] - \frac{\alpha}{(1-2\nu)} \Delta T. \quad (1.12c)$$

On the contrary, in order to find the relationship between stress and strain in the plane stress problem, equation (1.8) is substituted in equation (1.10)

$$\sigma_x = \frac{E}{(1-\nu^2)} [\epsilon_x + \nu\epsilon_y] - \frac{\alpha}{(1-\nu)} \Delta T, \quad (1.13a)$$

$$\sigma_z = \frac{E}{(1-\nu^2)} [\nu\epsilon_x + \epsilon_y] - \frac{\alpha}{(1-\nu)} \Delta T. \quad (1.13b)$$

1.1.3. Thermo-optic Simulation Theory

The optic processes where thermal energy exists can result significant nonlinear effects. The origin of the nonlinearity might be the incident laser power itself absorbed when it passes through the material and a heater mounted on the waveguide. The change in the temperature affects the refractive index of the material as well. For gases, the refractive index typically decreases with increasing temperature (at constant pressure), but for condensed matter its refractive index can either increase or decrease with changes in temperature, depending upon details of the internal structure [34].

The temperature and the refractive index are related. Thermal effect is mathematically described as follows

$$n = n_0 + \left(\frac{\partial n}{\partial T} \right) (T - T_0) \quad (1.14)$$

where n is the final refractive index, n_0 is the initial refractive index, $\frac{\partial n}{\partial T}$ is the thermo-optic coefficient, T is the final temperature, and T_0 is the initial temperature. The quantity of $\frac{\partial n}{\partial T}$ shows dependency of the refractive index, n to a material given and the $(T-T_0)$ indicates the change of the temperature in the waveguide. It should be noted that the thermal effects often cause a strong time-dependent nonlinear optical phenomenon, even though the change of the temperature is quite long (in seconds).

Chapter 2

Model & Method

The Finite Element Method (FEM) has developed into a key, indispensable technology in the modelling and simulation of advanced engineering systems in various fields like housing, transportation, communications, and so on. In building such advanced engineering systems, engineers and designers go through a sophisticated process of modelling, simulation, visualization, analysis, designing, prototyping, testing, and lastly, fabrication. Note that much work is involved before the fabrication of the final product or system. This is to ensure the workability of the finished product, as well as the cost effectiveness. The process is illustrated as a flowchart in Figure 2.1. This process is often iterative in nature, meaning that some of the procedures are repeated based on the results obtained at a current stage, so as to achieve an optimal performance at the lowest cost for the system to be built. Therefore, the techniques related to modelling and simulation in a rapid and effective way play an increasingly important role, resulting in the application of the FEM being multiplied numerous times because of this. Brief information about the software used for the simulations is given and the technical details such as mesh, boundary conditions etc. about them will be discussed in this section [35].

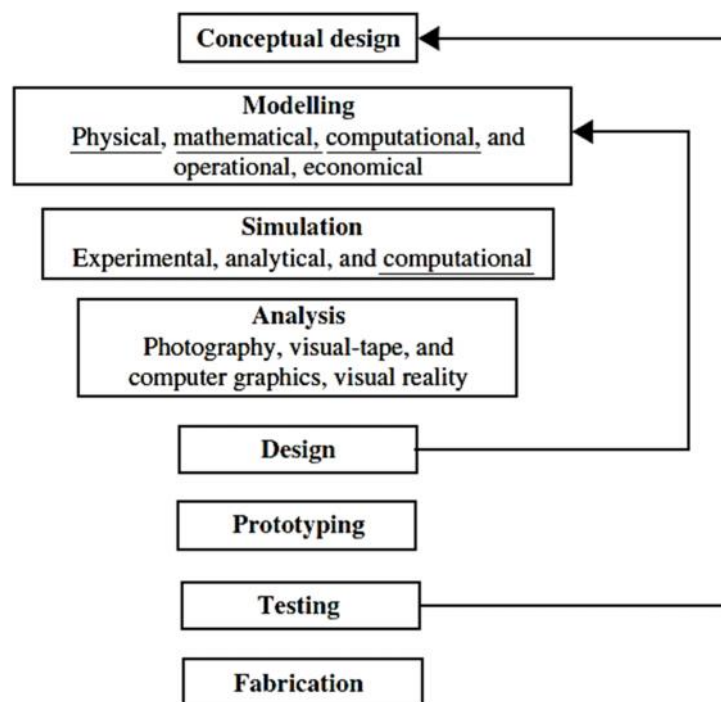


Fig. 2.1 Processes leading to fabrication of advanced engineering systems. [35]

2.1. What is FEATool Multiphysics?

It is the abbreviation of “Finite Element Analysis Toolbox for Multiphysics” and contains physics, finite element analysis (FEA), and partial differential equation (PDE) simulation toolbox [36]. The simulations from the numerous fields in physics such as heat transfer, fluid

dynamics, chemical engineering, structural mechanics, fluid-structure interaction (FSI), and electromagnetics can be fully modeled. The physics modules embedded in the software can be used or a PDE equation can be customized via FEATool in 1D, 2D, or 3D [37]. Six buttons which are located in the upper side of the left panel of the main window of the software FEATool as shown in figure 2.2. This main graphical user interface (GUI) window is used in the modeling process. FEATool is employed and used by the academic researchers for, [38] [39] teaching, [40] [41] and also in the industrial engineering simulation works [42].

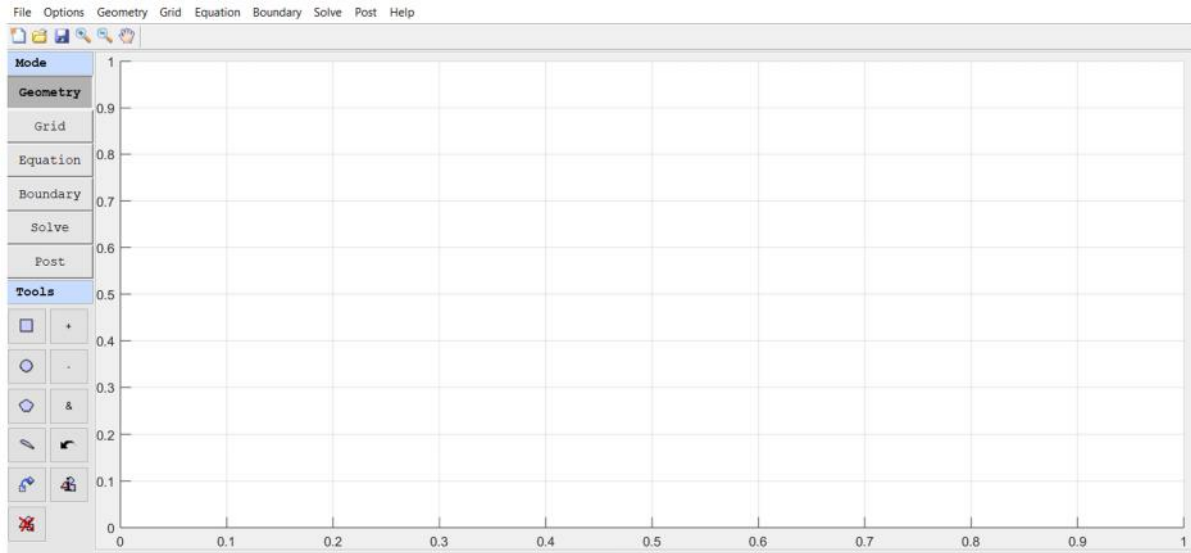


Fig. 2.2: Main graphical user interface (GUI) window

In addition, FEATool fully integrates state-of-the-art open source solvers such as FEniCS, OpenFOAM, and SU2, external mesh generators Gmsh, Netgen, and Triangle, and the post-processing and visualization tools ParaView and plotly. This enables anyone to use these solvers and simulation tools without much effort, which otherwise would take a significant time to understand and learn how to use [43]. Figure 2.2 shows the steps of the model processing.

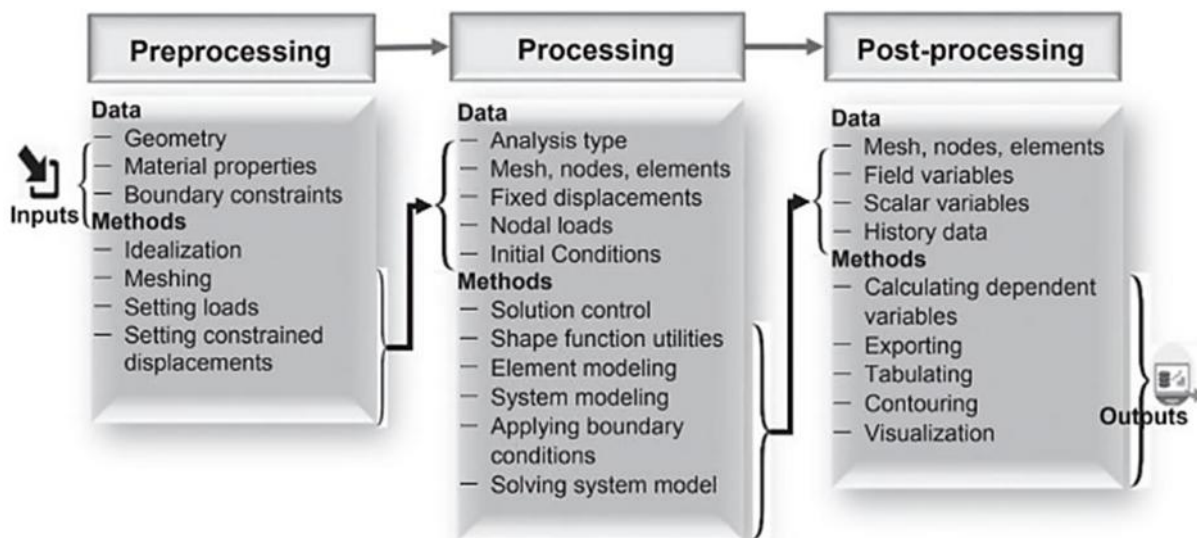


Fig. 2.3: Typical data and methods in the procedure of finite element analysis modeling [35]

2.2. Multiphysics Mode

The equations and coefficients are defined for each domain of the model. Numerous equations are pre-defined for many topics as the ones, heat transfer and plain stress that are used in the simulations. Also, FEATool allows to describe and enter the customized the equations manually.

FEATool Multiphysics is a fully integrated physics and PDE simulation environment where the modeling process is subdivided into six steps; preprocessing (CAD and geometry modeling), mesh and grid generation, physics and PDE specification, boundary condition specification, solution, post-processing, and visualization [44].

The simulations for heat transfer and stress analysis in the project are made simultaneously by FEATool under the mode called as multiphysics environment which is the combination of heat transfer and plain stress modules in this study. Now, the steps made before running the simulations will be explained.

2.2.1. Selecting the Dimension

The models are made as 2-dimension (2D) which don't require a very advance computer and a large memory space.

2.2.2. Geometrical Design

This is the step where the shape of the model is created by the geometrical objects such as rectangles, circles, blocks, and cylinders. Also, more complex shapes can be formed by extracting or adding the objects each other.

Two models are chosen to be examined. Model 1 shown in figure 2.4 where the microheater with 20 μm height and 1200 μm width was placed at the top of the waveguide. The core was chosen as PMMA material with 40 μm width and 1600 μm width, the cladding as monomer with 20 μm height and 1600 μm width. Model 2 is shown in figure 2.5 where the microheater had a 20 μm height and 1200 μm width. The heater is buried inside the middle of the top cladding. It is also made up of the polysilicon material. The core is chosen as PMMA material with 40 μm height and 1600 μm width. The cladding as monomer had an 80 μm height and 1600 μm width. The coordinate system starts from the bottom left corner which is taken as (0, 0) for the x- and z- axis. The shorter side is taken as x-axis and the longer side where also the light propagates is the z-axis.

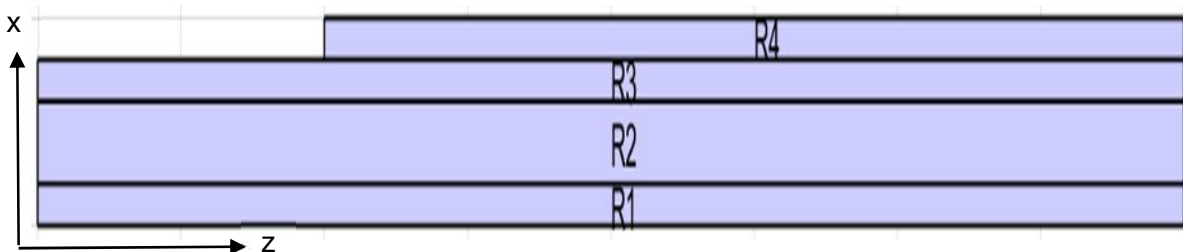


Fig. 2.4: Geometry of model 1

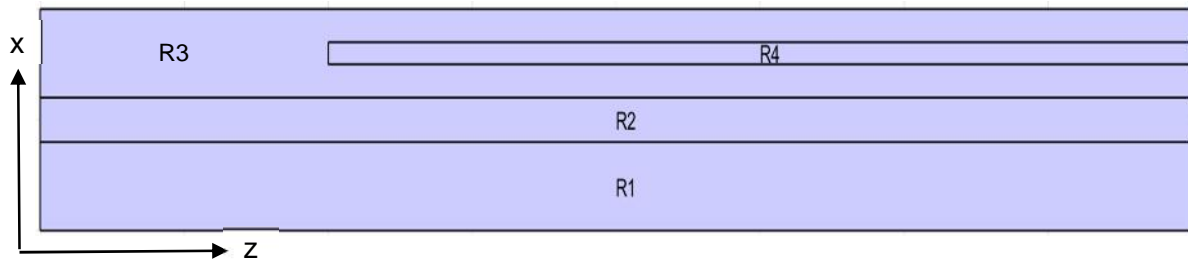


Fig. 2.5: Geometry of model 2

2.2.3. Mesh Generation

Mesh can be generated for the domains created in geometry or imported models. The fast and efficient 2D mesh and grid generator, Triangle, by J.R. Shewchuk's is fully integrated with FEATool Multiphysics [45][46][47]. Advantages of using Triangle compared to other built-in grid generation functions is firstly the overall speed, as it is one of the fastest 2D unstructured mesh generators available (completely written in C code). Moreover, Triangle features better support for specifying the grid size in different subdomains and geometry regions, as well as on boundaries, allowing for greater flexibility and higher quality grids adapted to specific problems and geometries [48].

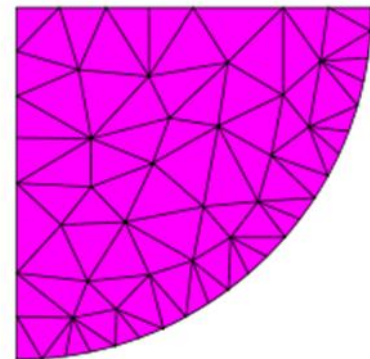


Fig. 2.6: An example of unstructured grid for a finite element analysis mesh

Figure 2.6 shows an example of unstructured grid for a finite element analysis mesh where Triangle method by J.R. Shewchuk's is used.

The denser or finer grids lead to a more accurate solution. The information from two neighboring points on the domain might be the same or not distinguishable if the mesh is not set well. In order to get the most accurate results for the parameters needed (e.g. Temperature, stress, strain, deformation). The grid size of the models shown in the previous part is chosen as 6.1×10^{-6} m which is smallest possible in the software. Figure 2.7. a, model 1 and 2.7. b, model 2 show the meshes.

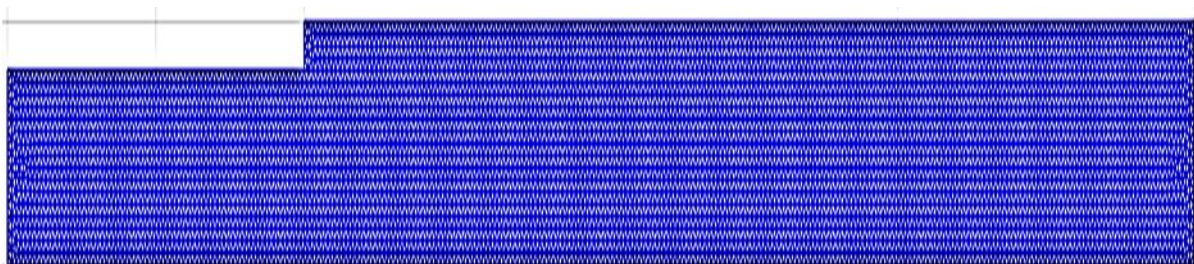


Fig. 2.7. a: Mesh of model 1



Fig. 2.7. b: Mesh of model 2

2.2.4. Definition of the Equations

Equations (PDEs) and model coefficients are specified in subdomain/equation mode to describe the physical phenomena to be modeled. Equations are pre-defined for many types of physical phenomena like for example heat transfer, structural strains and stresses, and fluid flow. In addition, FEATool also allows arbitrary and custom systems of PDE equations to be described and entered [49]. Now, the equations used for the simulations in this project will be explained.

Heat is transferred by the conduction for our case. Therefore, we extracted the parts for convection and radiation from the equation. We used the Mathematical equation below in the thermal simulation is

$$\rho C_p T' + \nabla (-k \nabla T) = Q \quad [50] \quad (2.1)$$

where T is the temperature, ρ is the density, C_p is the specific heat, and k is the thermal conductivity. T_0 is the initial temperature at each point of the waveguide which is taken as 20 °C. The parameters used in the simulation are as followed

	[kg/m ³]	C_p [J/kg*°C]	k [W/m*°C]
Monomer	940	1890	0.147
PMMA	1190	1500	0.25
Microheater (Polysilicon)	2320	678	34

Table 1: The parameters used in the thermal simulation

Mathematical equations are used as below for the plain stress simulation.

$$u - E / (1 - \nu^2) ((u_x + \nu_y - (1 + \nu) T) + (1 - \nu) / 2 (u_y + \nu_x)) = 0, \quad (2.2a)$$

$$v - E / (1 - \nu^2) ((\nu u_x + v_y - (1 + \nu) T) + (1 - \nu) / 2 (u_y + \nu_x)) = 0 [51] \quad (2.2b)$$

Here, ρ is the density, u is the displacement along the x axis, E is the Young's modulus, ν is the Poisson's ratio, v is displacement along the y axis, α is the thermal expansion coefficient, T is the temperature. Initial temperature is considered as 20 °C. The left and the right sides of the models in Fig. 1 are fixed in the simulation. The parameters used in the simulation are as followed.

	[kg/m ³]	E [GPa]		[K ⁻¹]
Monomer	940	3.3	0.40	72.22 e-6
PMMA	1190	2.76	0.37	22.25 e-6
Microheater (Polysilicon)	2320	160	0.22	2.6 e-6

Table 2: The parameters used in the stress and deformation analysis

RF module in COMSOL multiphysics software with the appropriate boundary conditions is used to make the optical simulation. Also, we used the heat transfer module simultaneously in order to see the effect of temperature on the index of refraction. The equation below is used to make the simulation of the mode analysis and get the effective modal index.

$$\nabla^2 E_t + \nabla \left(\frac{\nabla n^2(x,y) E_t}{n^2(x,y)} \right) + \left(\frac{2\pi}{\lambda} \right)^2 n^2(x,y) E_t = \left(\frac{2\pi}{\lambda} \right)^2 n_{eff} E_t \quad [52] \quad (2.3)$$

derived from Maxwell's equations, where E_t is the transverse electric field, λ is the wavelength, $n(x,y)$ is the refractive index distribution and n_{eff} is the effective index (wave equation eigenvalue). The initial refractive index, n_o of the core and cladding are taken as 1.4885 and 1.412 respectively.

2.2.5. Boundary Conditions

They must be prescribed on the geometrical boundaries to account for interactions with the surroundings outside of the modeled domain. For time dependent problems initial conditions must also be given at the start of the simulations. Figure 2.8 and 2.9 illustrates the boundaries for the upper and buried microheater models and the boundary conditions used in the softwares will be explained for each simulation.

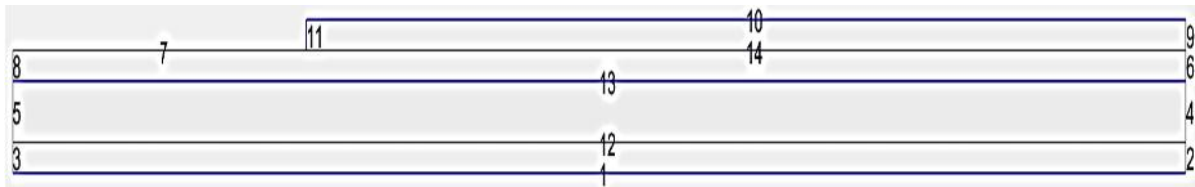


Fig. 2.8: Boundaries of model 1

The boundary conditions for the heat transfer module are set as $T = T_0$ for all the boundaries related to monomer and PMMA materials, numbered from 1 to 8 in figure 2.8 and 1 to 5, 7, 8, 9, 10, in figure 2.9 and $T = T_{microheater}$ for the microheater for the boundaries numbered as 9, 10, 11, and 14 in the first figure and 6, 13, 14, and 15 in the second figure. Interior boundaries of the claddings and the core numbered as 12 and 13 in the first model and 11 and 12 in the second model are set as continuity which accepts the core and the cladding parts as whole for the heat transfer.

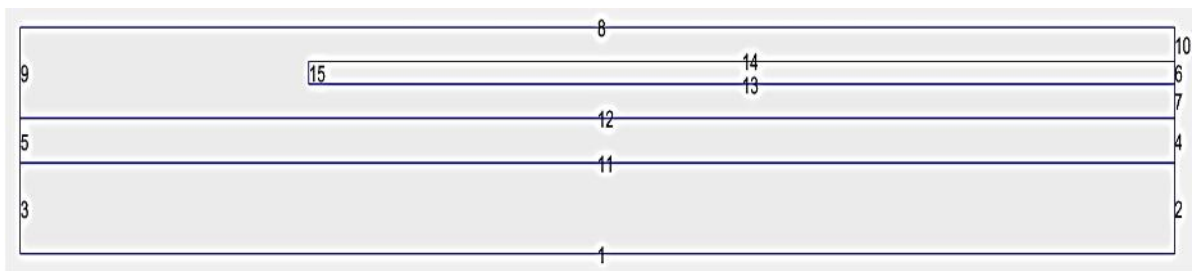


Fig. 2.9: Boundaries of model 2

The boundary conditions for the plain stress module are made for the upper microheater model. In order to get the boundaries on the left and the right sides of the waveguide shown in figure 2.7 fixed, the displacements of the boundaries 2, 3, 4, 5, 6, 8, and 9 are set as u and v for x - and z - axis. Hence, the waveguide is not able to elongate in the left or right directions.

Impedance boundary condition for RF module of the optical simulation is applied to boundary 5 in figure 2.8 in order to mode analysis.

2.2.6. Solving/Computing of the Problem

In the previous steps, the problem is specified completely. Now, a suitable solver mentioned in the first part of this chapter can compute the discretized system and solve the simultaneous equations for the field variables at the nodes of the mesh. This is the most computer hardware demanding process. Different software packages use different algorithms depending upon the physical phenomenon to be simulated. There are two very important considerations while selecting an algorithm for solving a system of equations: one is the storage required, and another is the CPU (Central Processing Unit) time needed [53]. FEATool does this work either by default MATLAB linear solvers or use an external one such as FEniCS, SU2 CFD, or OpenFOAM solvers.

2.2.7. Visualization/Postprocessing of the Result

The digital data which is obtained by solving the equation in the previous section is usually a large volume. The results have to be visualized in such a way that it is easy to interpolate, analyze and present. The visualization is performed through a so-called post-processor, usually packaged together with the software. This the place where any information such as temperature, deformation etc. for any point or a 2D cut line chosen can be obtained. The object can be displayed in the form of wire-frames, group of elements, and groups of nodes. The user can rotate, translate and zoom into and out from the objects. Field variables can be plotted on the object in the form of contours, fringes, wire-frames and deformations. Usually, there are also tools available for the user to produce iso-surfaces, or vector fields of variable(s). Tools to enhance the visual effects are also available, such as shading, lighting and shrinking. Animations and movies can also be produced to simulate the dynamic aspects of a problem. Outputs in the form of tables, text files and x - y plots are also routinely available. [53] The examples can be seen in the last chapter of the report.

Chapter 3

Results

The project outcomes for the simulations will be presented in this section.

3.1. Thermal Simulation

Heat transfer module with appropriate boundary conditions in FEATool multiphysics software is used to make the simulation which is explained in the previous chapter. Thermal simulation is performed on the models for the different temperatures from 20 °C to 200 °C and the time range until the thermal equilibrium is reached in the fiber optic. Line 1(L1) is along the central axis of the core where the analysis of temperature, stress, and the refractive index are made. Figure 3.1. a and b illustrate the models, those were used in the simulations.

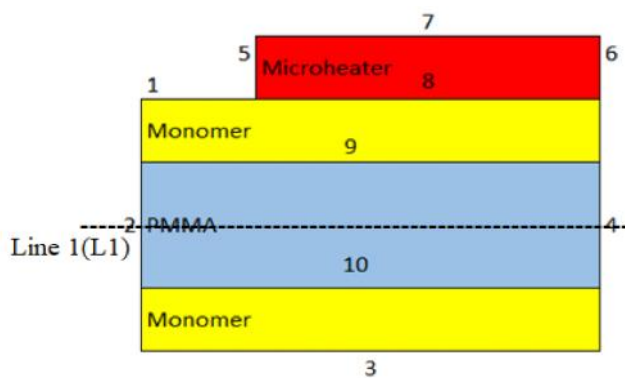


Fig. 3.1. a: Model 1

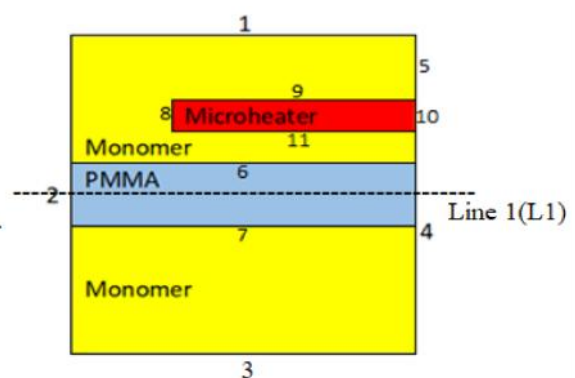


Fig. 3.1. b: Model 2

It is seen in video 3.1.a and video 3.2.a that the heat energy propagates through the waveguide in the downward direction until the thermal equilibrium is established for both of the models.



Video 3.1. a: Thermal distribution for model 1



Video 3.1. b: Thermal distribution for model 2

The points as a reference in the core along L1 at the coordinates, (1000 μm , 40 μm) and (1000 μm , 100 μm) for the models respectively are chosen at the right down position of the mid-point of the microheater in order to observe the temperature change over the time. The figure 3.2. a and b illustrate it. From the data which is obtained for the time increments of 0.25 ms for the first and 0.1 ms for the second models. It is interesting that even though, the models have all the materials same except the design, they don't have the same temperature profile. For the first model, the profile has an increase in temperature for 3.75 ms until 108 °C. The change is not significant after this point for 3 ms until the thermal equilibrium is established which is at 110 °C. This happens at 6.75 ms \pm 0.25 ms. Temperature increases for 4.3 ms until 141 °C for model 2. The changes after this temperature are not significant and achieved the equilibrium. It is only 2 °C increase for 2.7 ms until the thermal equilibrium which is 143.688 for the model. This occurs at 7 ms \pm 0.1 ms. This model's temperature profile changes uniformly between 0.7 ms and 1.9 ms. The change is about 5 °C for each 0.1 ms time increment.

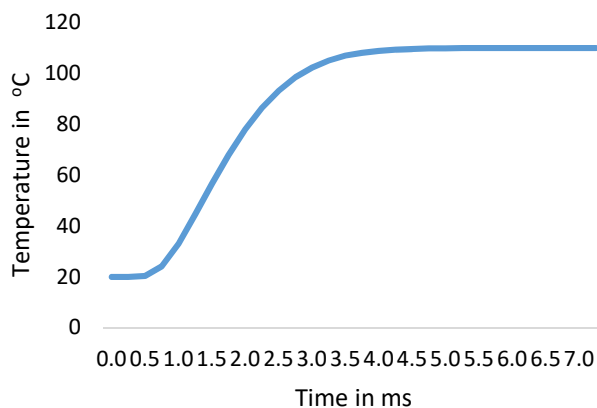


Fig. 3.2. a: Temperature-Time graph for model 1

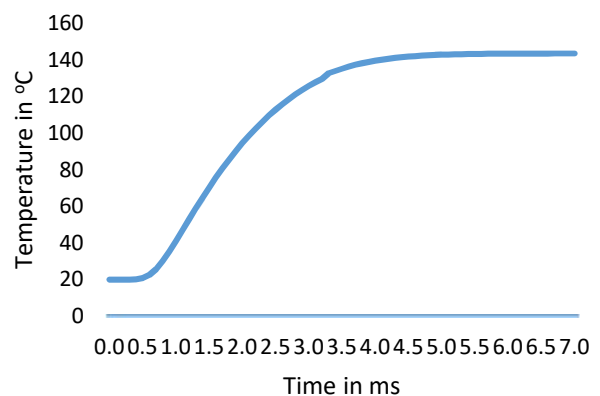


Fig. 3.2. b: Temperature-Time graph for model 2

In figure 3.3 blue and orange lines represent the model 1 and the model 2 respectively which show the temperatures along L1 where there is a sharp inclination in the temperatures for the microheater at the top and in the other hand, uniformly temperature distribution can be obtained where the heater is buried. The temperature distribution in vertical direction is gradient and inhomogeneous, because the microheater is only on one side of the waveguide.

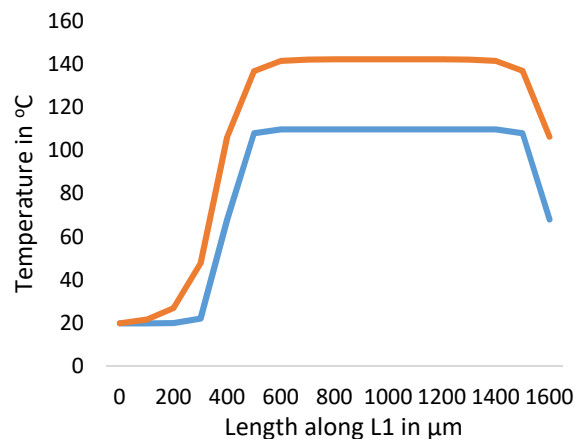


Fig. 3. 3: Thermal distribution along L1 for model 1 and model 2

Figure 3.4. a and b show the thermal distributions for the polymer waveguides when the microheater is placed at the top and inside the upper cladding, respectively. The temperatures on the temperature contours along the line which is perpendicular to L1 and the propagation are obtained for the line from the mid-point of the microheater. Note that the x axis and the z axis have different scales. The dark red color and the dark blue color in the color scheme indicate the highest and the lowest temperatures respectively and the room temperature is equal to 20 °C.

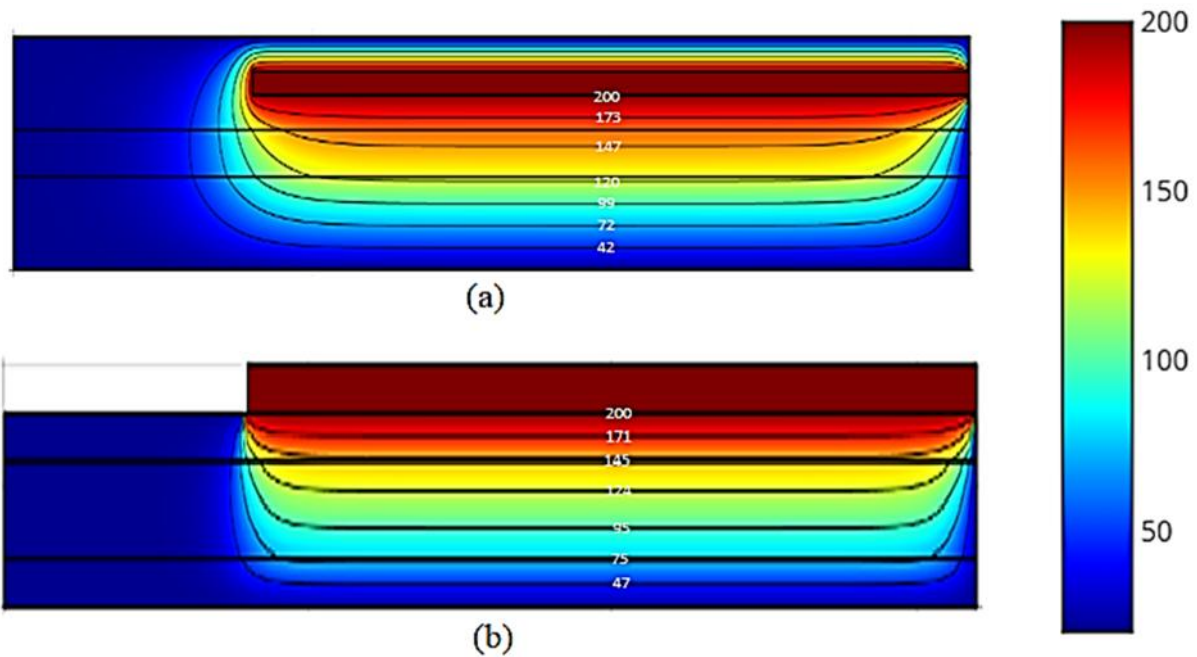


Fig. 3. 4 a and b: Temperature distributions for model 1 and model 2

3.2. Stress and Deformation Analysis

Stresses can cause anisotropic and inhomogeneous distribution of the refractive index. [23] Commercially available Finite Element Analysis solver software by FEATool Multiphysics was utilized to get generated stress and the modulation solves the stress and the modulation in the index of refraction for the waveguide. The data about the stress is obtained by FEATool Multiphysics plain stress module with proper boundary conditions for the models which are shown in the figure 3.5. a and b.

Dark red color and dark blue color show the maximum and the minimum deformations regions in the waveguide respectively and the red arrows indicate the magnitude and the direction of the deformation. On the left and the right sides, the deformation occurs very slightly in the downward direction and very strongly in the upward direction from the middle in the first model. In the second model, the waveguide is stretched in the downward direction from the left and the right side very slightly and in the upward direction from the middle part profoundly. The scales of the models in the figures are exaggerated by the tool in the software in order to see the deformation effects in the regions of the waveguides clearer.

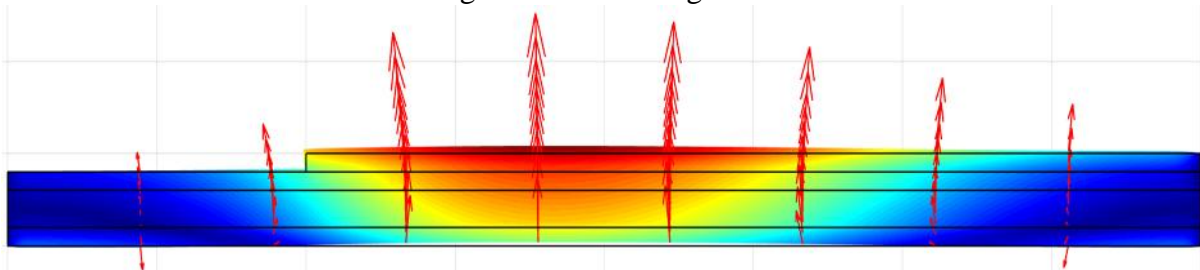


Fig. 3.5. a: Deformation distribution for model 1

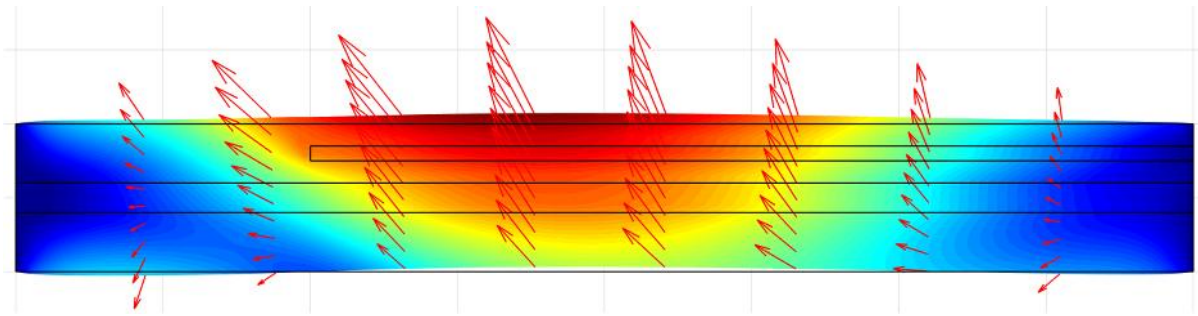


Fig. 3.5. b: Deformation distribution for model 2

In the deformation analysis, it is obtained in the plain stress simulation where the left and the right sides of the waveguides are fixed that the waveguides are deformed by 831.29 nm and 488.112 nm in the y axis respectively which are shown in figure 3.6. a and b.

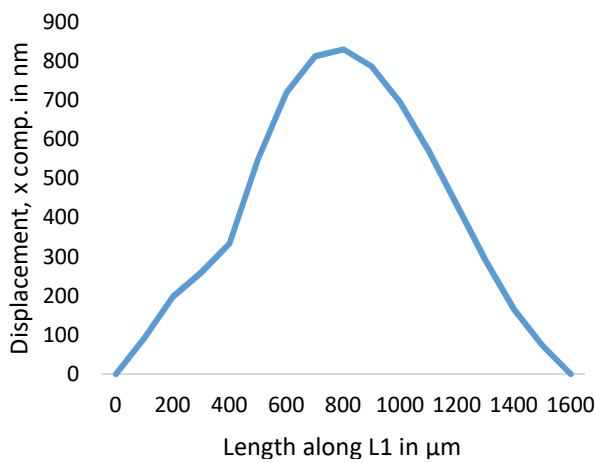


Fig. 3.6. a: Displacement-Length graph in x-axis for model 1

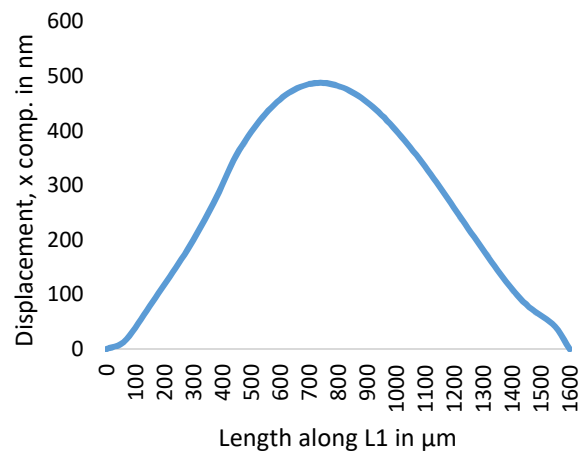


Fig. 3.6. b: Displacement-Length graph in x-axis for model 2

The left sides of the waveguides are fixed only to find the maximum possible elongations along L1 which reaches to the maximum values of 1.4 μm and 1.62 μm respectively. It is shown in figure 3.7. a and b. The right sides of the waveguides are free to get elongated.

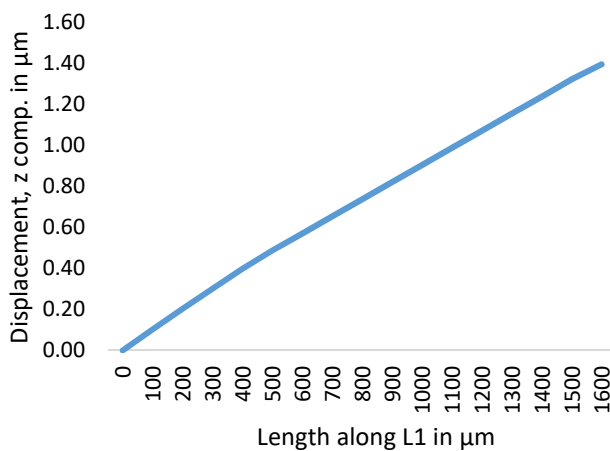


Fig. 3.7. a: Displacement-Length graph along L1 for model 1

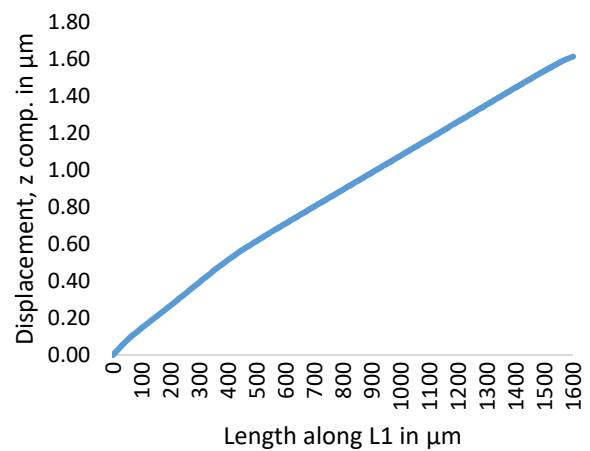


Fig. 3.7. b: Displacement-Length graph along L1 for model 2

In figure 3. 8. a and b and figure 3. 9. a and b, it can be inferred that refractive index and stress act dependently. In order to find it out, the relationship between the change in the refractive indices, Δn and stress along L1 are examined for the both of the models at 200 °C respectively. This relationship can be seen where the changes are marked by the red circles. It is found that they have a strong negative correlation. This is valid for the models both. But it is not noticeable in the second model as profound as the first one.

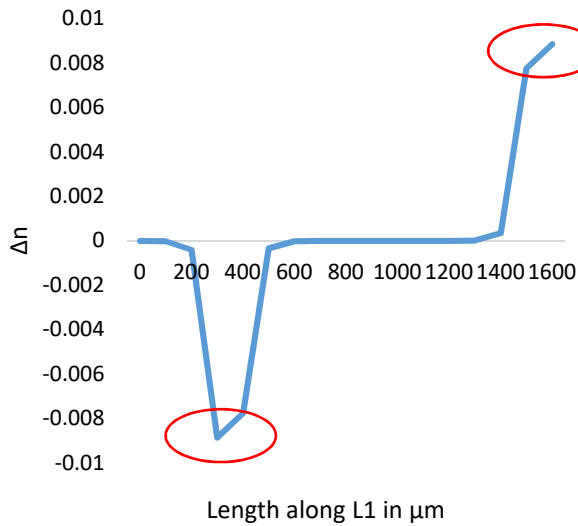


Fig. 3. 8.a: Refractive index change-Length graph along L1 for model 1

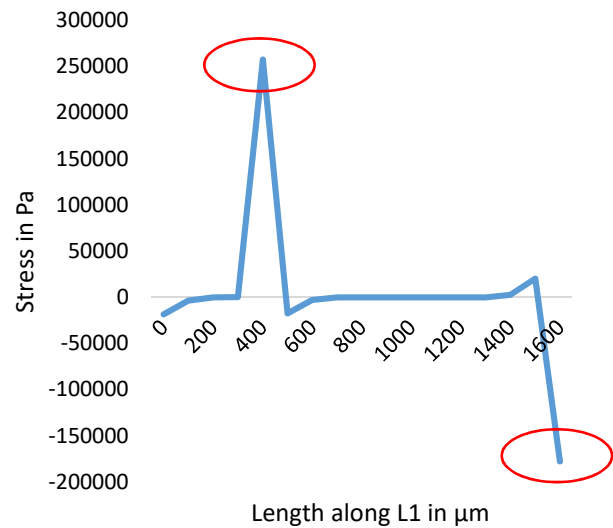


Fig. 3. 8.b: Stress-Length graph along L1 for model 1

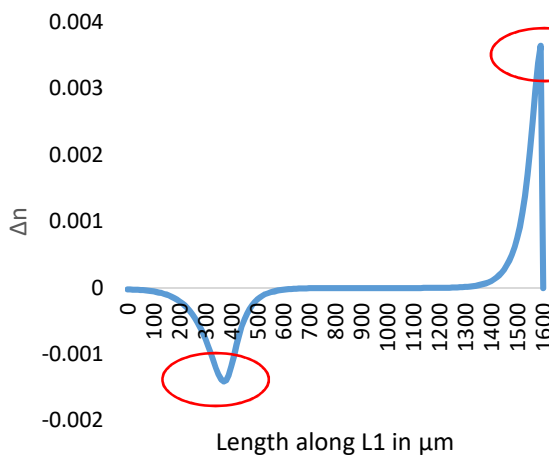


Fig. 3. 9. a: Refractive index change-Length graph along L1 for model 2

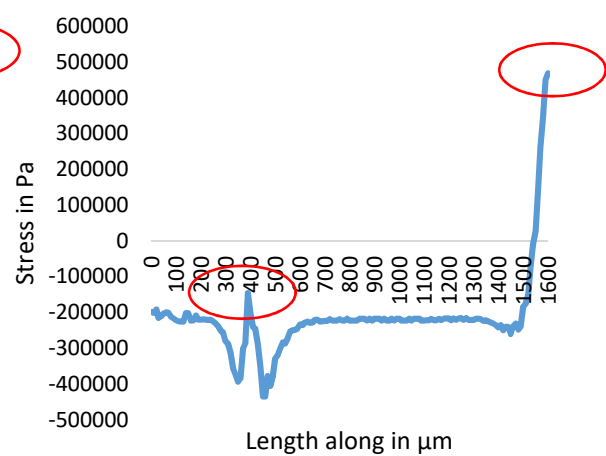


Fig. 3. 9. b: Stress-Length graph along L1 for model 2

3.3. Thermo-Optic Simulation and Analysis

RF module in COMSOL multiphysics software with the impedance boundary condition is used to make the optical simulation. Also, we used the heat transfer module simultaneously in order to see the effect temperature on the index of refraction. The data is obtained for TEM mode analysis as shown in figure 3.10. a and b. The results showed that a noticeable difference does not exist on the waveguide by temperature. Therefore, the initial values are taken here. It is not seen by a bare eye. But the difference can be seen in the effective mode indices of TEM modes. The effective mode index values for electric field and magnetic field are 1.1676 V/m or A/m before heating 1.11322 V/m or A/m after the heating. The TEM modes with and without the temperature are shown as same in the figures.

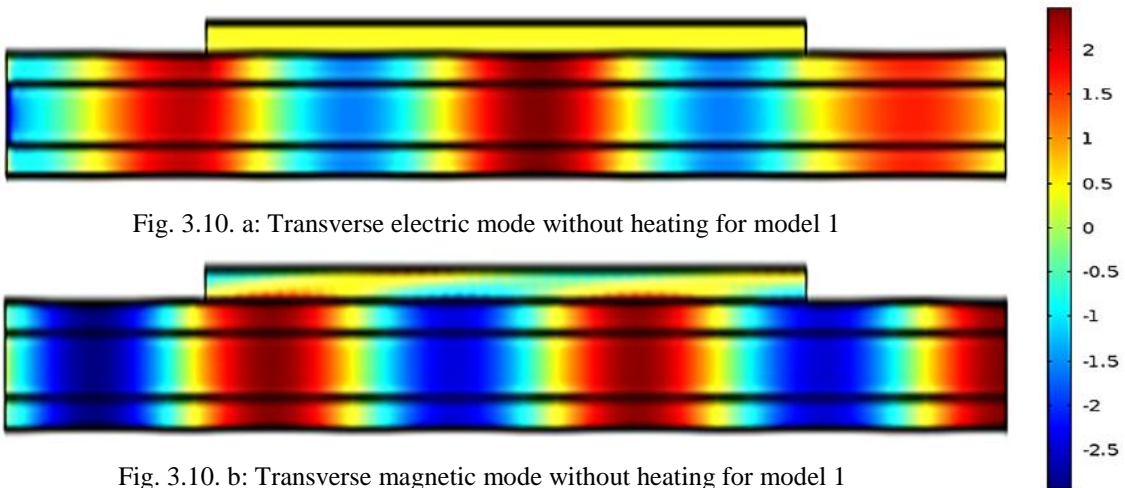


Figure 3.11. a and b illustrate the change in the refractive indices of the core and the cladding for both of models of the waveguides which are induced by the temperature. As it is mentioned in the thermal simulation part that the thermal distribution is uniform for the buried microheater and this lowers the index of refraction more compared to model 1.

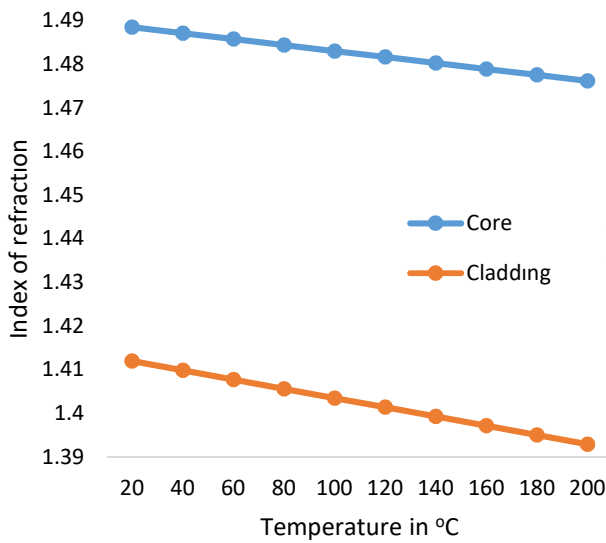


Fig. 3.11. a: Refractive Index-Temperature graph for the core and the cladding for model 1

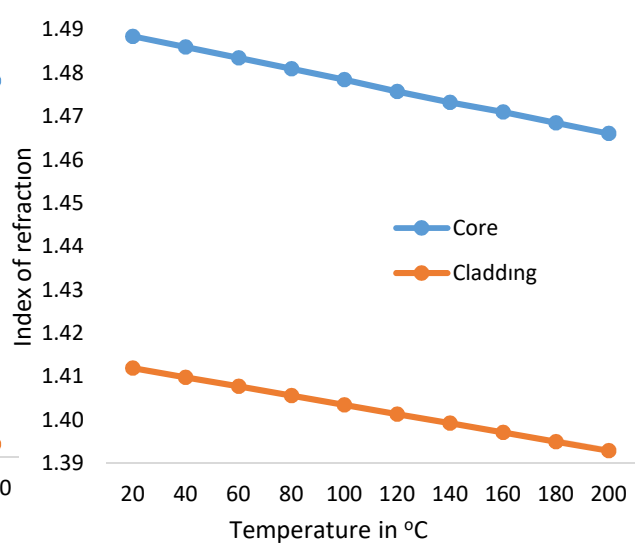


Fig. 3.11. b: Refractive Index-Temperature graph for the core and the cladding for model 2

Chapter 4

Conclusion

The thermal analysis, the stress analysis, and the optical characteristics of polymer waveguides where the microheater is mounted at the top for the first model and inside the upper cladding for the second model are studied in this work.

Temperature gradient is observed for the first model and the core and the surrounding regions and the waveguide is heated uniformly in the second model. This shows that the buried model is much suitable and faster for the heating uniformly. Also, the model is ideal to be used between 25 °C and 90 °C. The temperature of the core increases uniformly in this range.

The deformation is less in the buried model than model 1. Also, stress is not effective on this model as much as model 1.

The refractive index decreases by temperature for both of the models. The refractive index can be tuned in the broader range for model 2 than model 1.

Because of the reasons stated above, the second model is preferred to be used for a waveguide. The model can serve as the platform for optical integration. The tunable Bragg filter can be realized by it [54]. Also, it can be used for the tunable lasers.

This study has similar results to [55] in temperature distribution, [12] in T-t graph, [56] in temperature contour distribution, [57] and [13] in refractive index change.

References

- [1] Eldada L, Shacklette LJ. *Sel Top Quantum Electron* 2000; 6:54–67.
- [2] Zhou M. *Opt Eng* 2002; 41:1631–43.
- [3] Jang C, Chen RT. *J Lightwave Technol* 2003; 21:1053–8.
- [4] Siebel U, Hauffe R, Bruns J, Petemann K. *Photonics Technol Lett* 2001;13:957–79.
- [5] Noh Y, Lee C, Kim J, Hwang W, Won Y, Lee H, et al. *Opt Commun.* 2004; 242:533–40.
- [6] Lu Y, Guo H, Wang H, Chi S. *Microwave Opt Technol Lett* 2003;39:1–3.
- [7] Ahn S, Shin SJ. *Sel Top Quantum Electron* 2001; 7:819–25.
- [8] Ma C, Zhang H, Zhang D, Cui Z, Liu S. *Opt Commun* 2004;241:321–2.
- [9] Keil N, Yao HH, Zawadzki C. *Appl Phys B: Lasers Opt* 2001;73:619–23.
- [10] Zhiyi Zhang , Ping Zhao, Peng Lin, Fengguo Sun *Polymer* 47 (2006) 4893–4896.
- [11] N. Keil, H. H. Yao, and C. Zawadzki, “Athermal polarization independent arrayed-waveguide grating (AWG) multiplexer using an all-polymer approach,” *Appl. Phys. B* 73, 619–622 (2001).
- [12] M. M. Rahman and M. F. Hossain, "Thermal performance analysis of polymer optical waveguides for thermo-optic applications," 2014 9th International Forum on Strategic Technology (IFOST), Cox's Bazar, 2014, pp. 65-68.
- [13] S N Kasarova et al 2010 *J. Phys.: Conf. Ser.* 253 012028
- [14] Schott, A. G. (2017). Optical glass—collection datasheets. Homepage: <http://www.us.schott.com/advancedoptics/english/products/opticalmaterials/optical-glass/optical-glass/index.html>.
- [15] Pfeffer M 2010 *Handbook of plastic optics* ed S Baumer (New York: Wiley–VCH) p 23
- [16] Nishihara, H., M. Haruna, and T. Suhara. 1989. *Optical Integrated Circuits*. New York: McGraw-Hill Book Co.
- [17] Gorachand G 1998 *Handbook of optical constants of solids* ed E D Palik (London–Academic Press) p 118
- [18] Hauffe, R., & Petermann, K. (2006). *Thermo-Optic Switching*.

- [19] Changbao Ma, Edward R. Van Keuren, "Simulations of thermo-optic effects in beam propagation," Proc. SPIE 5595, Active and Passive Optical Components for WDM Communications IV, (25 October 2004)
- [20] T. Goh, Proc. SPIE 4582, 49 (2001).
- [21] S. Toyoda, N. Ooba, Y. Katoh, T. Kurihara, T. Maruno, *Electr. Lett.* 36, 1803 (2000).
- [22] Xu and Stroud, 1992; Sapriel, 1979
- [23] Huang, M. (2003). Stress effects on the performance of optical waveguides.
- [24] Moller, B. A., L. Jensen, C. Laurent-Lund, and C. Thirstrup. 1993. Silica-Waveguide Thermo-optic Phase Shifter with Low Power Consumption and Low Lateral Heat Diffusion. *IEEE Photonics Technology Letters.* 5(12): 1415-1418.
- [25] Sircilli, F., M. A. R. Franco, A. Passaro, and N. M. Abe. 2001. Finite Element Analysis of Thermo-Optic Integrated Photonic Devices. *IEEE IMOC Proceedings.* 329-332.
- [26] Wang Weyl-kuo, H. J. Lee, and P. J. Anthony. 1996. Planar Silica-Glass Optical Waveguides with Thermally Induced Lateral Mode Confinement. *IEEE Journal of Lightwave Technology.* 14(3): 429-436.
- [27] Kokkas, A. G. 1974. Thermal Analysis of Multiple-Layer Structures. *IEEE Transactions on Electron Devices.* ED-21(11): 674-681.
- [28] Changbao Ma (2007), Modeling of thermo-optic switches (Master's thesis).
- [29] Jiji, L. M. (2013). Heat transfer essentials: A textbook.
- [30] Turner, M. J., R. W. Clough, H. C. Martin, and L. J. Topp. 1956. Stiffness and deflection analysis of complex structures. *J. Aero. Sci.* 23:805-823.
- [31] Kawachi, M. 1990. Silica waveguide on silicon and their application to integrated-optic components. *Opt. and Quantum Electron.* 22:391-416.
- [32] Okamoto, K. (2000). Fundamentals of optical waveguides.
- [33] Timoshenko, S. and J. N. Goodier. 1951. *Theory of Elasticity.* New York: McGraw-Hill.
- [34] André, P., Rocha, A.M., Domingues, F., & Facão, M. (2011). Thermal Effects in Optical Fibres.
- [35] Bi, Z. Finite element analysis applications.
- [36] FEM Multiphysics Simulation for MATLAB (engineer.com).
- [37] Engineering - FEM Multiphysics Simulation for MATLAB (engineering.com).
- [38] Modeling the Effects of Increased Glucose Concentration on Intraocular Pressure CSURE 2014 Summer Program (PDF).

- [39] Multiple Scale Modeling for Predictive Material Deformation Analysis (PDF).
- [40] The Department of Civil Engineering at the University of Memphis CIVIL 7117 course notes.
- [41] Department of Mathematics at Lamar University course notes.
- [42] Topology Optimization Modeling with MATLAB and FEATool Multiphysics.
- [43] Simulation, P., 2020. Precise Simulation - Physics Simulation Made Easy.
- [44] Shewchuk, J., 2020. Triangle: A Two-Dimensional Quality Mesh Generator and Delaunay Triangulator.
- [45] J.R. Shewchuk, Triangle: Engineering a 2D Quality Mesh Generator and Delaunay Triangulator, in *Applied Computational Geometry: Towards Geometric Engineering* (Ming C. Lin and Dinesh Manocha, editors), volume 1148 of *Lecture Notes in Computer Science*, pages 203-222, Springer-Verlag, Berlin, May 1996. (From the First ACM Workshop on Applied Computational Geometry).
- [46] J.R. Shewchuk, Delaunay Refinement Algorithms for Triangular Mesh Generation, *Computational Geometry: Theory and Applications* 22(1-3):21-74, May 2002.
- [47] Unstructured MATLAB 2D Mesh and Grid Generation using Triangle | FEATool.
- [48] Topology Optimization Modeling with MATLAB and FEATool Multiphysics.
- [49] Hysing , J. S. (2019, July 10). FEATool Multiphysics. Retrieved February 12, 2020, from <https://www.featool.com/doc/physics.html>
- [50] M.B.J. Diemeer/ *Optical Materials* 9 (1998) 195
- [51] Johan S. H, Featool Multiphysics Plain Stress Physics v. 1.11 / 24 July 2019 [Computer software]
- [52] Passaro, V. M. N. and Leonardis, F. De, [Recent Advances in Modelling and Simulation of Silicon Photonic Devices, Modelling and Simulation], I-Tech Education and Publishing, 367-390 (2008)
- [53] Liu, G., & Quek, S. The finite element method.
- [54] Zhang, Z., Liu, D., Felipe, D. de, Liu, A., Keil, N., and Grote, N., Polymer embedded silicon nitride thermally tunable Bragg grating filters, submitted to *Appl. Phys. Lett.* (2013).
- [55] Zhang, Z., Zhao, P., Lin, P., & Sun, F. (2006).
- [56] Zhang, Z., & Keil, N. (2016). Thermo-optic devices on polymer platform.

[57] Anjin Liu, Ziyang Zhang, Dongliang Liu, Norbert Keil, and Norbert Grote. Thermo-optic simulations of silicon nitride / polymer hybrid waveguides.